Published in final edited form as:
J Mol Biol. 2008 March 14; 377(1): 193–205. doi:10.1016/j.jmb.2007.12.046.

The ATPase cycle mechanism of the DEAD-box rRNA helicase, DbpA

Arnon Henn[1,*], **Wenxiang Cao**[1,*], **David Hackney**[2], and **Enrique M. De La Cruz**[1,†]

1*Yale University, Department of Molecular Biophysics & Biochemistry, 260 Whitney Avenue, New Haven, CT 06520*

2*Carnegie Mellon University, Department of Biological Sciences, 4400 Fifth Avenue, Pittsburgh, PA 15213*

Summary

DEAD-box proteins are ATPase enzymes that destabilize and unwind duplex RNA. Quantitative knowledge of the ATPase cycle parameters is critical for developing models of helicase activity. However, limited information regarding the rate and equilibrium constants defining the ATPase cycle of RNA helicases is available, including the distribution and flux of populated biochemical intermediates, the catalytic step(s) that limits the enzymatic reaction cycle, and how ATP utilization and RNA interactions are linked. We present a quantitative kinetic and equilibrium characterization of the rRNA-activated ATPase cycle mechanism of DbpA, a DEAD-box rRNA helicase implicated in ribosome biogenesis. rRNA activates the ATPase activity of DbpA by promoting a conformational change after ATP binding that is associated with hydrolysis. Chemical cleavage of bound ATP is reversible and occurs via a gamma phosphate attack mechanism. ADP-P_i and RNA binding display strong thermodynamic coupling, which causes DbpA-ADP-P_i to bind rRNA with > 10-fold higher affinity than with bound ATP, ADP or in the absence of nucleotide. The rRNA-activated steady-state ATPase cycle of DbpA is limited *both* by ATP hydrolysis and P_i release, which occur with comparable rates. Consequently, the predominantly populated biochemical states during steady-state cycling are the ATP- and ADP-P_i-bound intermediates. Thermodynamic linkage analysis of the ATPase cycle transitions favors models in which rRNA duplex destabilization is linked to strong rRNA and nucleotide binding. The presented analysis of the DbpA ATPase cycle reaction mechanism provides a rigorous kinetic and thermodynamic foundation for developing testable hypotheses regarding the functions and molecular mechanisms of DEAD-box helicases.

Keywords

DEAD-box protein; RNA; helicase; ATPase; kinetics; nucleotide

Introduction

RNA helicases are ATPase enzymes that destabilize and unwind double-stranded RNA structures, refold RNA and disrupt RNA-protein complexes[1 - 4]. RNA helicases that belong to the superfamily II of molecular motor helicase enzymes known as DEAD- or the related

†Address correspondence to Enrique M. De La Cruz, Yale University, Department of Molecular Biophysics & Biochemistry, P.O. Box 208114, New Haven, CT, 06520-8114. Tel. (203) 432-5424; Fax. (203) 432-1296; email: enrique.delacruz@yale.edu.
*These authors contributed equally to this work.

DExH/D-box proteins[5], which are present in every organism from viruses to humans and play fundamental roles in viral transcription and replication, protein translation, proper pre-mRNA splicing and editing, ribosome biogenesis, RNA export to the cytoplasm, and RNA degradation[6]. Recent work has provided insight to the mechanism of DEAD-box helicase destabilization and unwinding[7 - 9], but the RNA-activated ATPase cycle and its linkage to duplex destabilization and unwinding has for the most part remained uncharacterized.

Detailed mechanistic studies of DEAD-box RNA helicases have been hindered by a requirement for additional regulatory subunits, leaky ATPase activity in the absence of RNA, and low RNA substrate specificity[10]. DbpA is non-processive ATP-dependent [7] helicase that destabilizes and unwinds short rRNA duplexes [11]. DbpA is unique among the *E. coli* DEAD-box family in that its ATPase activity is specifically activated by the peptidyl-transferase center (PTC) of the 23S ribosomal RNA[12], thus it provides a unique model system in which to examine enzymatic activation by RNA. DbpA is not activated by 5S rRNA, 16S rRNA, tRNA, native 50S or native 70S ribosomes, but is activated by denatured 70S ribosomes[13], favoring a physiological role in ribosome biogenesis and/or assembly.

It is well established that many classes of nucleic acid helicases couple the free energy from catalytic cycles of ATP binding, hydrolysis and product release to mechanical work in the form of nucleic acid duplex unwinding[14; 15] and translocation[16]. However, limited information is available regarding the ATPase cycle of RNA helicases, including the rate and equilibrium constants defining the enzymatic reaction cycle, the distribution and flux of populated biochemical intermediates, what catalytic step(s) limits catalytic cycling, and how ATP utilization and RNA interactions are linked[17; 18]. In particular, it is unclear how RNA binding increases the DEAD-box protein ATPase activity, which can be achieved by accelerating ATP binding, hydrolysis, and/or product release.

We present in this study a quantitative kinetic and equilibrium characterization of the rRNA-activated ATPase cycle mechanism of DbpA. The experimental approach and analysis employed allows us to define in quantitative terms *a*) the ATPase cycle reaction pathway, *b*) the distribution of populated biochemical intermediates, *c*) the free energy changes associated with individual ATPase cycle transitions, *d*) the biochemical reaction(s) that limit ATP utilization, *e*) the nucleotide and RNA binding linkage (i.e. how binding of one affects the other), and *f*) how the catalytic ATPase activity of DbpA is activated by rRNA. Quantitative knowledge of the rRNA-dependent ATPase cycle of DbpA will serve as the basis for developing mechanistic models of how ATP utilization is coupled to RNA helicase activity. Given the high homology among all identified prokaryotic and eukaryotic DEAD-box helicases, the detailed analysis of the DbpA ATPase cycle reaction mechanism provides a rigorous kinetic and thermodynamic foundation from which testable hypotheses regarding the functions and molecular mechanisms of DEAD-box helicases can be developed.

Results

Steady-state ATPase activity of DbpA

The ATPase activity of DbpA is accelerated >500-fold from <0.01 s^{-1} to ~5 s^{-1} by PTC-RNA under our experimental conditions (Figure 1). The Michaelis constant (K_m) for ATP in the presence of saturating PTC-RNA is 65 μM and the apparent Michaelis constant for 153-mer PTC-RNA in the presence of saturating ATP is 1.0 nM (Table 1), comparable to published values measured under slightly different conditions[12].

DbpA exists as a non-associating monomer in the absence[19] and in the presence of PTC-RNA, during both equilibrium conditions[19] and steady state ATP cycling[12]. We present evidence below that two distinct DbpA-ADP states exist when bound to PTC-RNA. Therefore, the

minimum reaction scheme that accounts for ATPase activity (ATP binding, hydrolysis and product release) free in solution and when bound to RNA, assuming that product release is sequential and P_i dissociation precedes ADP release, is defined by ten biochemical states, fifteen equilibrium, and thirty rate constants (Scheme 1). We use this reaction scheme as a framework for interpreting the transient kinetic experiments described in the following sections. We have omitted the non-specific collision complexes[20], which almost certainly exist, because they were not characterized in this study. We provide in the Appendix the explicit solution of the differential equations describing the formation and loss of the biochemical intermediates depicted in Scheme 1, and the equations used to analyze the kinetics of ATP binding, hydrolysis and product release measured in this study.

Nucleotide binding

The fluorescent mant-analogs were used to measure ATP and ADP binding to DbpA and DbpA-PTC complex. Previous measurements demonstrate that even though the mant fluorophore slightly alters the kinetics and affinity of unlabelled nucleotides ~2-fold[21], mant-nucleotides can be used to reliably monitor DbpA-nucleotide binding.

Time courses of fluorescence change after mixing DbpA with mantATP (Figure 2B) or mantADP[21] follow single exponentials with observed rate constants that depend linearly on the [mant-nucleotide] (Figure 2C and 3B), consistent with simple one-step binding mechanisms[21], yielding association rate constants from the slopes (k_{+T} = 1.4 μM^{-1} s^{-1} and k_{+D} = 3.3 μM^{-1} s^{-1}), dissociation rate constants from the intercepts (k_{-T} = 101 s^{-1}; k_{-D} = 170 s^{-1}) and overall equilibrium binding affinities from the ratio of rate constants (K_T = 72 μM and K_D = 51 μM; Table 1). The mantADP affinity (K_D) is comparable to published values measured with mantADP[21] or radiolabelled ADP[22]. The DbpA-mantADP dissociation rate constant (k_{-D}) measured directly by competition with unlabeled ADP is 130 s^{-1} (data not shown and[21]), comparable to the value obtained from the intercept of Figure 3B. The mantADP dissociation rate constant was unaffected by 100 mM P_i (data not shown), suggesting that the affinity of P_i for DbpA-ADP is >100 mM.

Time courses of fluorescence change after mixing DbpA-PTC with mantATP or mantADP are biphasic and follow double exponentials (Figure 2A, 2B, 3A), indicating that binding is monitoring at least two biochemical transitions. We favor a sequential, two-step binding mechanism (Scheme 1) over a parallel reaction pathway with binding to a mixed population because the relative amplitudes of the two phases measured in association (Figure 3A) and dissociation (Figure 3D; described below) reactions differ[23]. Accordingly, the fast observed rate constants (k_{fast}) are dominated by nucleotide binding and the slow observed rate constants (k_{slow}) arise from an isomerization(s) subsequent to nucleotide binding. We assume that the two high fluorescence states have similar intensities, so the observed fluorescence reflects the sum of the concentrations of these two species. The experimentally observed rate constants are independent of the relative intensities of these states, so the outcomes of the analysis presented below are unaffected if this assumption does not apply. The 2′- and 3′-mant nucleotide isomers exist as an equilibrium mixture (60% 3′ isomer) that interconvert slowly with a half life of ~10 minutes at pH 7.5, 25 °C[24]. The two isomers may bind DbpA with different kinetics, yielding the biphasic time courses, so measurements were also done with 2′-deoxy isomers labeled at the 3′ hydroxyl. The fluorescence changes associated with 2′-deoxymantATP binding are considerably smaller than with mixed 2′- and 3′- labeled isomers (data not shown), but the time courses remain biphasic, require a sum of two exponentials to describe the data, and are qualitatively similar, as reported for Rep DNA helicase[24].

The fast observed rate constant (k_{fast}) values depend linearly on the [mant-nucleotide] (Figure 2C and 3B). The fast phase is much more rapid than the slow phase in the case of mantATP binding (i.e. $k_{fast} \gg k_{slow}$; Figure 2). Under these conditions, $k_{fast} = k_{+RT}$[mantATP] + k_{-RT}

(Eq. 33 of Appendix), permitting the mantATP association rate constant (k_{+RT} = 1.2 μM^{-1} s^{-1}) and the dissociation rate constant (k_{-RT} = 61 s^{-1}) to be determined from the slope and intercept of the [mantATP]-dependence of k_{fast}, respectively (Figure 2C), and the mantATP binding affinity (K_{RT} = 51 μM) from the ratio of the rate constants (Table 1).

The slow phase observed with mantATP represents the approach to steady state following initial binding and has contributions from ATP hydrolysis (k_{+RH}), or more likely a conformational change preceding rapid ATP hydrolysis (these are kinetically equivalent), ATP resynthesis (k_{-RH}), and P_i release (k_{-RPi}). ADP release does not contribute the slow phase of ATP binding (Appendix) because it is more rapid than the preceding steps (discussed below). The limited [mantATP] range examined precludes reliable determination of the [mantATP]-dependence of the observed slow phase rate constant (k_{slow}). However, k_{slow} is predicted to depend hyperbolically on the [mantATP] (Eq. 34 of Appendix, discussed below) with a maximum observed rate constant at saturating [mantATP] that is equal to the sum of the ATP hydrolysis, ATP resynthesis and P_i release rate constants (k_{+RH} + k_{-RH} + k_{-RPi} ~11 s^{-1}, Fig. 2D). Measurements presented below with unmodified ATP (Figure 4B) confirm this prediction.

The $k_{fast} \gg k_{slow}$ condition is not fulfilled with mantADP binding to DbpA-RNA (Figure 3B). Consequently, the square root approximation[25] cannot be applied, so unconstrained global fitting of the [mantADP]-dependence of k_{fast} and k_{slow} (Figure 3B; Table 1) to the following quadratic rate constant equation(s)[23]:

$$k_{fast,slow} = \frac{(k_{+1RD}[ADP] + k_{-1RD} + k_{+2RD} + k_{-2RD}) \pm \sqrt{(k_{+1RD}[ADP] + k_{-1RD} + k_{+2RD} + k_{-2RD})^2 - 4(k_{-2RD}k_{-1RD} + k_{-2RD}k_{+1RD}[ADP] + k_{+2RD}k_{+1RD}[ADP])}}{2} \quad \text{(Eq. 1)},$$

was used to determine the mantADP binding (k_{+1RD} = 4.1 μM^{-1} s^{-1}), dissociation (k_{-1RD} = 137 s^{-1}), and isomerization (k_{+2RD} = 32 s^{-1}, k_{-2RD} = 77 s^{-1}) rate constants (Table 1). The corresponding mantADP binding (K_{1RD}) and isomerization (K_{2RD}) equilibrium constants calculated from the ratios of the rate constants are 33 μM and 2.4, respectively (Table 1).

The rate and equilibrium constants determined from the association time courses predict that the time course of irreversible mantADP release from an equilibrated DbpA-RNA-mantADP complex will be biphasic with a fast observed rate constant ($k_{off\text{-}fast}$) of ~190 s^{-1} and a slow observed rate constant ($k_{off\text{-}slow}$) of 55 s^{-1} according to the following equation(s)[23]:

$$k_{off-fast,off-slow} = \frac{(k_{-1RD} + k_{+2RD} + k_{-2RD}) \pm \sqrt{(k_{-1RD} + k_{+2RD} + k_{-2RD})^2 - 4(k_{-2RD}k_{-1RD})}}{2} \quad \text{(Eq.2)}$$

Experimental time courses of irreversible mantADP release are biphasic with observed rate constants of 170 s^{-1} and 40 s^{-1} (Figure 3D), consistent with two high fluorescence DbpA-RNA-mantADP states (HRD and HRD') that exist in a reversible equilibrium (Scheme 1) defined by the rate constants determined from the association kinetics (Table 1). Inclusion of up to 100 mM P_i does not affect dissociation mantADP from DbpA-RNA (data not shown), suggesting that the affinity of P_i binding to DbpA-ADP-RNA is > 100 mM.

The overall affinity for ADP binding to DbpA-PTC-RNA ($K_{RD,\ overall}$), accounting for both DbpA-RNA-ADP states, calculated using the following expression [23]:

$$K_{RD,overall} = K_{1RD}\left(\frac{K_{2RD}}{1+K_{2RD}}\right) \quad \text{(Eq.3)}$$

is 23 μM. The overall affinity estimated from the [ADP]-dependence of the total transient kinetic time courses amplitudes (Figure 3A) yields a comparable value of 38 μM (data not shown).

ATP hydrolysis—Time courses of ATP hydrolysis by DbpA and DbpA-PTC-RNA were measured by chemical quench flow with ^{32}P-ATP and by HPLC with ATP. There is no detectable hydrolysis of ATP (up to 1 mM) by DbpA in the absence of PTC-RNA. In contrast, ATP is hydrolyzed in the presence of PTC-RNA, although no significant burst phase could be resolved (data not shown). The lack of product formation with DbpA supports the interpretation that hydrolysis of bound ATP does not occur in the absence of PTC-RNA and that the slow phase of mantATP binding, present with DbpA-PTC-RNA but absent from DbpA alone (Figure 2), arises from ATP hydrolysis (or more likely an isomerization preceding rapid hydrolysis). Sequential mixing experiments of transient P_i release presented below further support this interpretation.

P_i release—Time courses of P_i release after mixing DbpA-PTC-RNA with ATP (Figure 4A) display a distinct lag phase that is well described by an exponential with negative amplitude [20] followed by a linear, steady-state phase (Eq. 38 in Appendix). The observed lag phase represents the formation of (at least one) intermediate preceding P_i release on the approach to steady state turnover with a rate constant that is comparable or slower than P_i release, consistent with the lack of a burst phase in the time course of ATP hydrolysis measured by chemical quench-flow.

The steady state rate determined from the slope of the linear phase depends hyperbolically on the [ATP] and yields a K_m for ATP of 82 μM (Table 1; data not shown). The observed rate constant of the lag phase (k_{lag}) also depends hyperbolically on the [ATP] (Figure 4B). The hyperbolic [substrate]-dependence of k_{lag} eliminates mechanism in which the observed lag phase arises from an initial slow isomerization of the enzyme that limits productive ATP binding, consistent with the nucleotide binding measurements (Figure 2). The hyperbolic [ATP]-dependence of k_{lag} is approximated by (Eq. 34 in Appendix):

$$k_{lag} \approx \frac{k_{+RT}[ATP](k_{+RH}+k_{-RH}+k_{-RPi})+k_{-RT}k_{-RH}+k_{-RT}k_{-RPi}+k_{+RH}k_{-RPi}}{k_{+RT}[ATP]+k_{-RT}} \quad \text{(Eq. 4)}$$

which simplifies to the sum of the ATP hydrolysis (k_{+RH}), ATP resynthesis (k_{-RH}) and P_i release (k_{-RPi}) rate constants at saturating [ATP]:

$$k_{lag,\infty}=k_{+RH}+k_{-RH}+k_{-RPi} \quad \text{(Eq. 5)}$$

P_i release is irreversible in the presence of phosphate binding protein, so P_i rebinding does not contribute to the observed relaxations. The intercept (i.e. limit as [ATP] approaches 0, $k_{lag,0}$) is proportional to:

$$k_{lag,0}=\frac{k_{-RT}k_{-RH}+k_{-RT}k_{-RPi}+k_{+RH}k_{-RPi}}{k_{-RT}} \quad \text{(Eq. 6)}$$

The best fit of the [ATP]-dependence of k_{lag} to a hyperbola yields a maximum observed rate constant ($k_{lag,\infty}$) of 19.5 s^{-1} at saturating [ATP] and an intercept ($k_{lag,0}$) of 8.8 s^{-1}. The midpoint of the hyperbola (i.e. apparent K_d, Figure 4B) is equal to the ATP affinity (K_{RT}, Eq. 37 in Appendix) and yields a value of 86 μM, within a factor of 2 of that determined from the kinetics of mantATP binding (51 μM, Figure 2).

Time courses of P_i release after mixing saturating PTC-RNA (1 μM) with DbpA (0.8 μM) that had been mixed with saturating ATP (2 mM) and aged for various times (18 ms - 25 s) are superimposable (data not shown), independent of the ageing time, and identical to time courses of P_i release measured by mixing DbpA·PTC-RNA complex with saturating ATP (2 mM). That is, equilibrating DbpA with ATP up to 25 s does not bypass the observed lag phase in P_i release that arises from slow ATP hydrolysis (or a conformational change limiting rapid ATP hydrolysis) preceding steady-state ATP turnover. These data indicate that DbpA does not

hydrolyze bound ATP during the ageing time, either because it is very slow and/or the equilibrium constant for ATP hydrolysis favors ATP synthesis ($K_{RH} = k_{-RH}/k_{+RH} \gg 1$), consistent with the chemical quench flow measurements, and the conclusion that RNA activates the DbpA ATPase cycle by promoting an isomerization that allows chemical cleavage of bound ATP.

Isotope Exchange—We used oxygen isotopic exchange[26; 27] to determine the reversibility of the ATP hydrolysis reaction (k_{-RH}) in the presence of PTC-RNA. If hydrolysis occurs without reversal ($k_{-RH} \ll k_{-RPi}$) then one and only one water-derived oxygen will be incorporated into the released P_i. Reversible resynthesis of ATP from ADP and P_i before release of P_i, however, can result in the incorporation of additional oxygen atoms from water into P_i. The partition coefficient

$$P_c = \frac{k_{-RH}}{k_{-RH} + k_{-RP_i}} \quad \text{(Eq. 7)}$$

for the fraction of DbpA-RNA-ADP-P_i that partitions back to DbpA-RNA-ATP can be calculated from the extent of incorporation of these extra water oxygens into the P_i[28]. For the ~50% enrichment of the water in ^{18}O as used here, hydrolysis without reversal will incorporate one water-derived oxygen per P_i and will thus yield equal amounts of the species with 0 and 1 ^{18}O per P_i and none of the species with 2, 3 or 4 oxygens per P_i (as indicated by the fit in Figure 5 at $P_c = 0$). The observation of a significant amount of the species with 2 ^{18}O per P_i with DbpA (Figure 5) indicates that reversal of hydrolysis does occur. A P_c value of 0.2 was obtained as the best fit to a random mode[28], which corresponds to a P_i release rate constant (k_{-RPi}) that is ~4 times faster than the ATP resynthesis rate constant (k_{-RH}).

Knowledge of the P_c value, $k_{lag,\infty}$ and $k_{lag,0}$ allow us to determine the values of the fundamental rate constants defining ATP hydrolysis, ATP resynthesis and P_i release using Eqs. 6-8. ATP hydrolysis (k_{+RH}) occurs at 11.9 s^{-1}, ATP resynthesis (k_{-RH}) occurs at 1.5 s^{-1} and P_i release (k_{-RPi}) occurs at 6.1 s^{-1}. The equilibrium constant for ATP hydrolysis determined from the ratio of the rate constants ($K_{RH} = k_{-RH}/k_{+RH}$) is 0.13 (Table 1).

PTC-RNA binding—The affinity of nucleotide-free DbpA for 153mer PTC-RNA (K_R in Scheme, 1) determined by electrophoretic mobility shift assay under our conditions is 16 nM (Table 1, data not shown), comparable to published values measured under slightly different buffer conditions [22]. The value of $K_{m,RNA}$ measured from [RNA]-dependent ATPase is determined by the K_d's for RNA binding to DbpA intermediate states populated during ATP cycling (Appendix). Therefore, comparison of the $K_{m,RNA}$ value with the affinity of RNA in the absence of nucleotide (K_R) provides information regarding the RNA affinity of populated cycling intermediates

If $K_{m,RNA} < K_R$, at least one nucleotide-bound intermediate that binds RNA more strongly than nucleotide-free DbpA must be populated during ATPase cycling. If $K_{m,RNA} > K_R$, at least one populated intermediate binds RNA more weakly than nucleotide-free DbpA. The PTC-RNA binding affinity in the absence of nucleotide (16 nM) is larger than the $K_{m,RNA}$ value measured during steady-state cycling (1 nM), indicating that at least one nucleotide-bound intermediate state(s) populated during steady-state cycling binds PTC-RNA with a higher affinity (< 16 nM) than nucleotide-free DbpA.

Knowledge of the affinities of nucleotide-free DbpA for PTC-RNA (K_R) and nucleotide for DbpA (K_T and K_D) and DbpA-PTC-RNA (K_{RT} and K_{RD}) provides the information required to explain in thermodynamic terms how nucleotide bound to DbpA modulates the RNA binding affinity and vice-versa (i.e. how the two binding sites are linked/coupled). Detailed balance allows the PTC-RNA affinity of DbpA with bound ATP to be calculated from $K_{TR} = K_R$

K_{RT}/K_T (Scheme 1, Table 1). The affinities of DbpA with bound ADP (K_{1DR} and K_{2DR}) or ADP-P_i (K_{PiR}) for PTC-RNA can be determined in a similar manner (Table 1).

Initial ATP or ADP binding weakly affects the affinity of DbpA for PTC-RNA and vice versa ($K_T \sim K_{RT}$, $K_D \sim K_{RD}$, and $K_R \sim K_{TR} \sim K_{1RD}$), indicating that RNA and ATP or ADP binding are weakly coupled in DbpA. DbpA with bound ADP-P_i binds PTC-RNA with a $\gg$10-fold higher affinity than nucleotide free DbpA or DbpA with bound ATP or ADP, revealing that strong allosteric RNA and nucleotide binding linkage exists when ADP-P_i is bound to DbpA. This observation suggests that DbpA-RNA with bound ADP-P_i is significantly populated during steady-state ATP cycling and contributes to the low $K_{m,RNA}$ value. We hypothesize that formation of an "activated", hydrolysis-competent, strong ATP binding state (omitted from Scheme 1 for simplicity) precedes and limits rapid chemical cleavage of the ATP γ-phosphate bond [29; 30; 31] and that this state resembles and behaves similar to DbpA-ADP-P_i with respect to the strong RNA binding affinity. The activated, ATP hydrolysis competent and post-hydrolysis ADP-P_i states of DbpA may be mimicked to some extent by AMPpNp binding, which increases the PTC-RNA binding affinity of DbpA[22], though more work needs to be done to confirm that DbpA-PTC with bound AMPpNp reliably mimics an on-pathway reaction intermediate.

Distribution of Biochemical States—Knowledge of the ATPase cycle rate and equilibrium constants permits determination of the steady-state distribution of the biochemical intermediates populated during ATP cycling (Figure 6). The predominantly populated intermediates under our experimental conditions are the ADP-P_i-bound (~53%) and the ATP-bound (~33%) states. The significant populated mole fraction of the ADP-P_i-bound state and it's high affinity for PTC-RNA explains why the $K_{m,RNA}$ value measured from steady-state ATPase cycling activity is smaller than the binding affinity in the absence of nucleotide (K_R). However, the distribution of biochemical states populated under *in vivo* nucleotide concentrations (ATP ~3 mM, ADP ~0.25 mM and P_i ~5 mM)[32] shifts to the ADP-bound state (~ 60%), with ADP-P_i- and ATP-bound states comprising a smaller fraction (~25% and ~15%, respectively) than under our experimental conditions, indicating that the weak RNA binding conformations of DbpA are predominantly (~75%) populated *in vivo*.

Discussion

DbpA ATPase activity and activation by PTC-RNA

PTC-RNA accelerates the maximum DbpA ATPase activity (k_{cat}) ~500-fold from <0.01 s^{-1} to ~ 5 s^{-1} (Table 1). Nucleotide (ATP and ADP) binding and dissociation from DbpA are very rapid (Table 1), indicating that ATP turnover by DbpA in the absence of PTC-RNA is limited by some other step(s) in the cycle (Scheme 1, top pathway) such as ATP hydrolysis and/or P_i release. Time courses of mantATP and mantADP binding to DbpA with bound PTC-RNA are biphasic, in contrast to only one phase in the absence of PTC-RNA. The observed fast phases reflect nucleotide binding and dissociation and are similar in the presence and absence of PTC-RNA (Table 1), indicating that PTC-RNA has minimal effects on nucleotide binding to DbpA; rather, PTC-RNA binding promotes an isomerization after ATP or ADP binding. The significance of the additional ADP binding state is unclear and because it is weakly populated (<10% mole fraction) during steady-state ATP cycling, we will not consider it further in this study. However, the slow phase observed with mantATP reflects ATP hydrolysis, ATP resynthesis, and P_i release, indicating that PTC-RNA activates the DbpA ATPase activity by promoting any or all of these transitions. The high DbpA-PTC-RNA binding affinities[22] (Table 1) and the rapid rates of rebinding (data not shown) implies that dissociation of the complex is negligible[22] during steady state cycling and that cycling exclusively along the lower pathway depicted in Scheme 1 when PTC-RNA is present.

PTC-RNA activates the steady-state ATPase activity of DbpA by shunting DbpA along a different ATP hydrolysis pathway (lower path in Scheme 1). In the absence of PTC-RNA, DbpA does not hydrolyze bound ATP to an appreciable extent, suggesting a slow, rate-limiting ATP hydrolysis that is accelerated by PTC-RNA. Alternatively, ATP hydrolysis by DbpA could be rapid, but the equilibrium largely favor the ATP state (i.e. ATP resynthesis is more rapid than hydrolysis and neither are rate limiting). Our data cannot distinguish between these two possibilities. Nonetheless, the outcome is the same: DbpA without bound PTC-RNA binds but does not hydrolyze ATP. Because both DbpA and DbpA-PTC-RNA bind ATP, but no hydrolysis occurs without RNA, PTC-RNA binding must induce conformational rearrangement of DbpA that allows ATP hydrolysis to occur. PTC-RNA may also modulate the rate of P_i release from DbpA. However, PTC-RNA activation of DbpA ATPase activity is achieved by promoting ATP hydrolysis, which does not occur significantly in its absence.

The PTC-RNA activated steady-state ATPase cycle of DbpA is limited *both* by a step after ATP binding (interpreted as a step preceding rapid ATP hydrolysis) *and* P_i release, which occur with comparable rates. ATP hydrolysis is readily reversible, but P_i release (~6 s^{-1}) occurs ~4-fold more quickly than ATP resynthesis (~1.5 s^{-1}). P_i release can be considered to be essentially irreversible since rebinding is slow and overall binding weak (Table 1). Slow ATP hydrolysis and P_i release causes the ATP- and ADP-P_i-bound intermediates to be predominantly populated during steady-state ATP cycling under our conditions (2 mM ATP, <10 μM ADP). However, the distribution favors population of the ADP-bound states under physiological nucleotide concentrations (~3 mM ATP, ~250 μM ADP).

The steady-state ATPase parameters (k_{cat}, $K_{m,ATP}$, and $K_{m,RNA}$) are defined in terms of individual ATPase cycle rate constants according to the following expressions (Eqs. 25, 26 and 55 of Appendix):

$$k_{cat} = \frac{k_{+RH}k_{-RPi}}{k_{+RH}+k_{-RH}+k_{-RPi}}$$
$$K_{m,ATP} = \frac{k_{-RT}k_{-RH}+k_{-RT}k_{-RPi}+k_{+RH}k_{-RPi}}{k_{+RT}\left(k_{+RH}+k_{-RH}+k_{-RPi}\right)}$$
$$K_{m,RNA} = \frac{\left(k_{-RH}+k_{-RPi}\right)K_{TR}+k_{+RH}K_{PiR}}{k_{+RH}+k_{-RH}+k_{-RPi}} \quad \text{(Eq. 8)}$$

The values of these parameters predicted from the experimentally determined rate and equilibrium constants are comparable to the experimentally determined values (k_{cat} predicted ~4 s^{-1}, observed ~5 s^{-1}; $K_{m,ATP}$ predicted ~23 μM, observed ~65 μM; and $K_{m,RNA}$ predicted ~5 nM, observed ~1 nM; Table 1), indicating that the applied model and analysis are valid, and that the experimentally determined rate and equilibrium constants are consistent with the overall steady-state ATPase cycling behavior of DbpA. When we account for the ADP (7 μM) present under our experimental conditions (Eq. 42 of Appendix), the predicted $K_{m,ATP}$ value increases slightly (~27 μM; Table 1), while the k_{cat} and $K_{m,RNA}$ are unaffected since they are independent of [ADP]. Under physiological nucleotide conditions (3 mM ATP, 250 μM ADP; Figure 6), the apparent $K_{m,ATP}$ increases dramatically to 190 μM due to competition with ADP, accounting for the shift in the distribution of populated ATP- and ADP-bound states (Figure 6).

Communication between RNA and nucleotide binding sites

PTC-RNA does not affect the affinity of DbpA for ATP or ADP, and as predicted from thermodynamic linkage, neither ATP nor ADP binding significantly affects the affinity of DbpA for PTC-RNA. That is, nucleotide (ATP and ADP) and PTC-RNA binding are weakly coupled. This does not mean that there are no nucleotide- or RNA-dependent conformational changes in DbpA. However, if significant conformational rearrangement of DbpA is coupled to nucleotide or PTC-RNA binding alone, these do not affect binding of the other ligand. The

structures of the DEAD-box protein, UAP56, with and without bound ADP[33] are consistent with small structural perturbations being coupled to nucleotide binding. There is no high resolution structure available of a DEAD-box protein with bound RNA and no bound adenine nucleotide. The weak coupling predicts that if the DbpA nucleotide binding site were perturbed by PTC-RNA binding, it would be in a way that does not affect initial ATP or ADP binding.

In contrast, strong thermodynamic coupling is displayed with ADP-P_i and RNA binding. DbpA with bound ADP-P_i binds PTC-RNA with > 10-fold higher affinity than in the absence of nucleotide, suggesting that DbpA undergoes significant conformational change when both RNA and ADP-P_i are bound. The high-resolution crystal structure of the Vasa DEAD-box protein with bound RNA and AMPpNp shows a closure of the nucleotide-binding cleft[34]. Binding of AMPpNp may mimic an intermediate populated after initial ATP binding and preceding P_i release, though the possibility that it represents an off-pathway intermediate cannot be eliminated. Therefore, it is likely that the conformational change that occurs after initial ATP binding to DbpA is a closure of the nucleotide-binding cleft separating the two RecA domains that comprise the DbpA helicase core domain[19; 35]. Cleft closure would promote non-covalent interactions between bound Mg^{2+} and ATP with the conserved helicase motifs across the cleft of the DbpA core domain[34], which would favor strong Mg^{2+} and ATP binding and formation of the ATP hydrolysis competent, strong PTC-RNA binding conformation (not shown in Scheme 1, discussed above). The hydrolysis-competent ATP state likely binds PTC-RNA and nucleotide with high affinity as does the post-hydrolysis, ADP-P_i conformation (Scheme 1).

Our analysis confirms previous quantitative equilibrium binding measurements revealing the weak coupling between ADP and PTC-RNA binding[22]. Strong coupling between ATP and PTC- RNA binding to DbpA was concluded from the same study[22]. However, as clarified by the authors, this conclusion was based on measurements done with AMPpNp, which binds differently than ATP[22]. DbpA with bound AMPpNp may better represent a chemical state populated *after* initial ATP binding (an activated ATP state omitted from Scheme 1 for simplicity, discussed below) and preceding product release.

ATPase cycle and free energy coupling

Unwinding of duplex RNA by DbpA is coupled to ATP utilization[2;19]. The ATP-dependence of efficient rRNA duplex unwinding by DbpA favors models in which destabilization and unwinding are coupled to one or more reaction steps along the DbpA ATPase cycle[7; 11]. Since nucleotide binding has minimal effects on PTC-RNA binding affinity (i.e. ATP and ADP binding processes are weakly coupled to PTC-RNA binding), it is very unlikely that large conformational rearrangement or unwinding of RNA occurs during initial ATP and ADP binding. On the other hand, the transiently populated DbpA-ADP-P_i state (and/or the strong ATP binding, hydrolysis competent state discussed above) binds rRNA ≫15-fold more strongly, indicating nucleotide-linked conformational rearrangement of the DbpA-PTC-RNA complex.

The free energy change associated with hydrolysis of ATP ($\Delta G^{o\prime}_{\text{hydrolysis}}$) in solution and at standard state is ~ -40 kJ mol^{-1} under our conditions[36]. In contrast, the total free energy change ($\Delta G^{o\prime}_{\text{tot}}$) associated with one catalytic turnover of ATP by DbpA-PTC-RNA, which reflects the sum of the free energy change for ATP hydrolysis (~ -40 kJ mol^{-1}) and the free energy change associated with work production[37], is < -0.5 kJ mol^{-1} ($\Delta G^{o\prime}_{\text{tot}} = \Delta G^{o\prime}_{\text{RT}} + \Delta G^{o\prime}_{\text{RH}} - \Delta G^{o\prime}_{\text{RPi}} - \Delta G^{o\prime}_{\text{2RD}} - \Delta G^{o}_{\text{1RD}}$; Table 2), considerably less than the value of $\Delta G^{o\prime}_{\text{hydrolysis}}$. The difference between $\Delta G^{o\prime}_{\text{hydrolysis}}$ and $\Delta G^{o\prime}_{\text{tot}}$ indicates that the hydrolysis free energy is transferred to and stored in the DbpA-PTC-RNA complex, suggesting that the final product is a high energy, DbpA-PTC-RNA complex in which the RNA is destabilized, unwound or unfolded and/or the DbpA is in a strained conformation. If the coupling efficiency is high and

used to disrupt RNA secondary structure, a single consumed ATP molecule could destabilize a maximum of 4-5 duplex RNA base pairs[38]. The reported 10-mer rRNA duplex unwinding rate constant of DbpA is much slower[39] (< 0.01 s^{-1}) than ATP turnover. The large difference suggests that futile (i.e. nonproductive) ATPase cycling occurs, presumably due to competitive reannealing of the partially unwound >4-5 base pair long segment.

We propose that the strong PTC-RNA binding transition is linked to rRNA duplex destabilization. The slow hydrolysis rate (i.e. large activation energy) and large PTC-RNA binding free energy change (Table 2) of this transition is consistent with significant conformational rearrangement of the DbpA-PTC-RNA complex. Consistent with the proposed destabilization mechanism, the high-resolution structure of the DEAD-box RNA helicase, Vasa[34], with bound ssRNA and AMPpNp undergoes a significant conformational change that favors closing of the nucleotide binding cleft and bending of ssRNA that precludes formation of Watson-Crick base pairing with a complementary strand. The observation that DbpA with bound AMPpNp strongly binds but does not unwind PTC-RNA duplexes[7] seems at variance with the proposed pathway. However, this observation can be accounted for if DbpA-AMPpNp populated a strong RNA binding state that destabilized short rRNA duplexes but did not dissociate the destabilized strands.

Scheme 1 and the experimental rate and equilibrium constants (Table 1) are consistent with strong PTC-RNA binding coinciding with an isomerization after ATP binding, interpreted as being a conformational change that precedes and limits ATP cleavage. Subsequent product release favors formation of the weak RNA binding conformation (Tables 1 and 2). Weak RNA binding enables DbpA to transfer the unwound rRNA product to other factors (e.g. the ribosomal proteins associated with the 50S subunit of the ribosome) and regenerate free DbpA capable of initiating another round of catalysis.

Materials and Methods

Reagents and Proteins

All chemicals and reagents were the highest purity commercially available. Millipore MlliQ® dispensed water that had been treated with DEPC for 8 hours and autoclaved was used in all procedures. RNAse activity was undetectable in all reagents, buffers and protein preparations. ATP (99+% purity as assayed by HPLC, data not shown) was purchased from Roche Molecular Biochemicals (Indianapolis, IN) and ADP (Sigma A-5285, 99+% purity by HPLC, data not shown) was purchased from Sigma (St. Louis, MO). Nucleotide concentrations were determined by absorbance using ε_{259} of 15,400 M^{-1} cm^{-1}. The *N*-methylanthraniloyl (mant) derivatives of ADP, 2′-deoxyADP, ATP, and 2′-deoxyATP were synthesized[23] and concentrations determined using ε_{255} of 23,300 M^{-1} cm^{-1}. A molar equivalent of $MgCl_2$ was added to nucleotides immediately before use.

DbpA was overexpressed and purified as described [2; 21]. The [DbpA] was determined by extinction coefficient method[21; 40]. MDCC (7-diethylamino-3-((((2- maleimidyl)ethyl) amino)carbonyl)coumarin)-labeled phosphate binding protein (P_iBiP) was expressed, purified and labeled as described[41].

RNA synthesis

A DNA fragment of 153 bp containing a sequence from the *E. coli* 23S rRNA (2454-2606 nt) was cloned into an Eco*RI* and Bam*HI* restriction site of (pTZ-18R). PTC-RNA was prepared by *in-vitro* transcription of Bam*HI* digested pTZ-18R-PTC with T7 RNA polymerase. Transcripts were treated with DNase I, phenol extracted (pH 4.7), passed through a G-50 mini-spun column (Roche Molecular Biochemical) and precipitated in ethanol. [RNA] were

calculated using ε_{260} = 8600 M^{-1} cm^{-1} $nucleotide^{-1}$. PTC-RNA was refolded[12] in 50 mM K-HEPES (pH 7.5), 50 mM KCl, 5 mM $MgCl_2$.

Steady state ATPase activity

The steady-state ATPase activity of DbpA (2-20 nM) was measured by absorbance (λ = 340 nm) using the ATP regenerating, NADH coupled assay [12; 42] at 25 (±0.1) °C in KMg75 buffer (75 mM KCl, 20 mM K-HEPES (pH 7.5), 5 mM $MgCl_2$, 1 mM DTT) supplemented with saturating (2 mM) ATP while varying the [PTC-RNA], or with saturating (120 nM) PTC-RNA and varying the [ATP]. The [RNA] or [ATP]-dependence of the steady state ATPase rate (V in units of ATP sec^{-1} $DbpA^{-1}$) was fitted to the quadratic form of the Briggs-Haldane equation:

$$V = k_o + (k_{cat} - k_o) \times \left(\frac{(K_m + [H]_{tot} + [S]_{tot}) - \sqrt{(K_m + [H]_{tot} + [S]_{tot})^2 - 4[H]_{tot}[S]_{tot}}}{2[H]_{tot}} \right) \quad \text{(Eq. 9)}$$

where k_o is the ATPase rate of DbpA alone, k_{cat} is the turnover rate at saturating [S], K_m is the *apparent* Michaelis constant for substrate activation, $[H]_{tot}$ is the total [DbpA], and and $[S]_{tot}$ is the total [PTC-RNA] or [ATP]. This equation assumes a 1:1 binding stoichiometry, which has been confirmed for PTC-RNA-activated ATPase activity of DbpA[12]. The [ADP] under our conditions of 2 mM ATP is ~7 μM [42].

Pre-steady state kinetic analysis

All transient kinetic fluorescence measurements were made in KMg75 buffer using an Applied Photophysics SX.18MV-R stopped-flow apparatus thermostatted at 25 ± 0.1 °C. The concentrations stated are final concentrations after mixing. Time courses were fitted to a sum of exponentials by nonlinear least squares fitting using Pro-K software provided with the instrument. Uncertainties are reported as standard errors in the fits unless stated otherwise.

Mant-nucleotide binding kinetics were measured by energy transfer from DbpA tryptophans (λ_{ex} = 280 nm) to bound mant-nucleotide (fluorescence monitored at 90° through a 400-nm long-pass colored glass filter) under pseudo-first order conditions with [nucleotide] ≫ [DbpA] or [DbpA-RNA][21]. Transient P_i release was measured using the fluorescently labeled mutant[43] of P_iBiP. Background P_i was removed from all solutions, syringes and the instrument with 7-methylguanosine (0.5-1 mM) and purine nucleoside phosphorylase (0.1 units mL^{-1}). There was ~5-fold enhancement in the fluorescence of MDCC-P_iBiP with P_i binding (λ_{ex} = 436 nm, 460 nm long pass emission filter). The rate and equilibrium constants of P_i binding to MDCC-P_iBiP under experimental conditions comparable to those used in this study are k_+ = 117 μM^{-1} s^{-1}, k_- = 24 s^{-1}, and K_d = 0.20 μM[41].

Time courses of [α-^{32}P]ATP hydrolysis were made at 25 °C in KMg75 buffer with a KINTEK (Austin, Texas) RQF-3 quench flow apparatus[31]. Experiments were done by mixing 23 μM DbpA or with 23 μM DbpA-PTC RNA 51mer with 20 μM ATP, ageing for various times then quenching with 5 M formic acid. Samples were spotted (2 μL) on a Cellulose F TLC plates (Analtech, Newark, DE) and resolved in 0.6 M KH_2PO_4 pH 3.4 for 45 min. Plates were exposed to phosphor screen, read using Storm PhosphorImager®, Molecular Dynamic (GE Healthcare), and quantitated using ImageQuant software, Molecular Dynamic (GE Healthcare). Formation of ADP from the hydrolysis of ATP (1 mM) by DbpA was also measured by HPLC[44].

Measurement of Oxygen Isotopic Exchange during ATP Hydrolysis

Hydrolysis of ATP was performed in KMg75 buffer containing 49% [^{18}O]-water supplemented with 2 mM ATP, 4 mM phosphoenolpyruvate, and 100 units mL^{-1} pyruvate kinase to regenerate

ATP. The reactions were quenched with acid and the P_i was isolated and analyzed for ^{18}O content[27].

Kinetic modeling

Simulations of reaction time courses and equilibrium distribution of biochemical states were performed with Tenua (provided by Dr. D. Wachsstock, available free at http://www.geocities.com/tenua4java/), which is based on the kinetic simulation program KINSIM developed by Carl Frieden and colleagues[45].

Supplementary Material

Refer to Web version on PubMed Central for supplementary material.

Acknowledgement

We thank Dr. Eckhard Jankowsky (Case Western Reserve) for comments on the manuscript. This work is supported by grants from the National Science Foundation (MCB-0546353), National Institutes of Health (GM071688), and American Heart Association (0655849T) to E.M.D.L.C. W.C. is supported by American Heart Association postdoctoral fellowship award 0625997T.

References

1. Cordin O, Banroques J, Tanner NK, Linder P. The DEAD-box protein family of RNA helicases. Gene 2006;367:17–37. [PubMed: 16337753]
2. Henn A, Medalia O, Shi SP, Steinberg M, Franceschi F, Sagi I. Visualization of unwinding activity of duplex RNA by DbpA, a DEAD box helicase, at single-molecule resolution by atomic force microscopy. Proc Natl Acad Sci U S A 2001;98:5007–5012. [PubMed: 11296244]
3. Mohr S, Matsuura M, Perlman PS, Lambowitz AM. A DEAD-box protein alone promotes group II intron splicing and reverse splicing by acting as an RNA chaperone. Proc Natl Acad Sci U S A 2006;103:3569–74. [PubMed: 16505350]
4. Fairman ME, Maroney PA, Wang W, Bowers HA, Gollnick P, Nilsen TW, Jankowsky E. Protein displacement by DExH/D “RNA helicases” without duplex unwinding. Science 2004;304:730–4. [PubMed: 15118161]
5. Linder P, Lasko PF, Ashburner M, Leroy P, Nielsen PJ, Nishi K, Schnier J, Slonimski PP. Birth of the D-E-A-D box. Nature 1989;337:121–2. [PubMed: 2563148]
6. Rocak S, Linder P. DEAD-box proteins: the driving forces behind RNA metabolism. Nat Rev Mol Cell Biol 2004;5:232–41. [PubMed: 14991003]
7. Diges CM, Uhlenbeck OC. *Escherichia coli* DbpA is an RNA helicase that requires hairpin 92 of 23S rRNA. Embo J 2001;20:5503–12. [PubMed: 11574482]
8. Yang Q, Jankowsky E. The DEAD-box protein Ded1 unwinds RNA duplexes by a mode distinct from translocating helicases. Nat Struct Mol Biol 2006;13:981–6. [PubMed: 17072313]
9. Tijerina P, Bhaskaran H, Russell R. Nonspecific binding to structured RNA and preferential unwinding of an exposed helix by the CYT-19 protein, a DEAD-box RNA chaperone. Proc Natl Acad Sci U S A 2006;103:16698–703. [PubMed: 17075070]
10. Linder P. Dead-box proteins: a family affair-active and passive players in RNP-remodeling. Nucleic Acids Res 2006;34:4168–80. [PubMed: 16936318]
11. Diges CM, Uhlenbeck OC. *Escherichia coli* DbpA is a 3′ -> 5′ RNA helicase. Biochemistry 2005;44:7903–11. [PubMed: 15910005]
12. Tsu CA, Uhlenbeck OC. Kinetic analysis of the RNA-dependent adenosinetriphosphatase activity of DbpA, an *Escherichia coli* DEAD protein specific for 23S ribosomal RNA. Biochemistry 1998;37:16989–96. [PubMed: 9836593]
13. Fuller-Pace FV, Nicol SM, Reid AD, Lane DP. DbpA: a DEAD box protein specifically activated by 23S rRNA. Embo J 1993;12:3619–26. [PubMed: 8253085]

14. von Hippel PH, Delagoutte E. A general model for nucleic acid helicases and their "coupling" within macromolecular machines. Cell 2001;104:177–90. [PubMed: 11207360]
15. Lohman TM, Bjornson KP. Mechanisms of helicase-catalyzed DNA unwinding. Annu Rev Biochem 1996;65:169–214. [PubMed: 8811178]
16. Tomko EJ, Fischer CJ, Niedziela-Majka A, Lohman TM. A nonuniform stepping mechanism for *E. coli* UvrD monomer translocation along single-stranded DNA. Mol Cell 2007;26:335–47. [PubMed: 17499041]
17. Lorsch JR, Herschlag D. The DEAD box protein eIF4A. 1 A minimal kinetic and thermodynamic framework reveals coupled binding of RNA and nucleotide. Biochemistry 1998;37:2180–93. [PubMed: 9485364]
18. von Hippel PH, Delagoutte E. Macromolecular complexes that unwind nucleic acids. Bioessays 2003;25:1168–77. [PubMed: 14635252]
19. Talavera MA, Matthews EE, Eliason WK, Sagi I, Wang J, Henn A, De La Cruz EM. Hydrodynamic characterization of the DEAD-box RNA helicase DbpA. J Mol Biol 2006;355:697–707. [PubMed: 16325852]
20. Robblee JP, Cao W, Henn A, Hannemann DE, De La Cruz EM. Thermodynamics of nucleotide binding to actomyosin V and VI: a positive heat capacity change accompanies strong ADP binding. Biochemistry 2005;44:10238–49. [PubMed: 16042401]
21. Talavera MA, De La Cruz EM. Equilibrium and kinetic analysis of nucleotide binding to the DEAD-box RNA helicase DbpA. Biochemistry 2005;44:959–70. [PubMed: 15654752]
22. Polach KJ, Uhlenbeck OC. Cooperative binding of ATP and RNA substrates to the DEAD/H protein DbpA. Biochemistry 2002;41:3693–702. [PubMed: 11888286]
23. Hannemann DE, Cao W, Olivares AO, Robblee JP, De La Cruz EM. Magnesium, ADP, and actin binding linkage of myosin V: evidence for multiple myosin V-ADP and actomyosin V-ADP states. Biochemistry 2005;44:8826–40. [PubMed: 15952789]
24. Moore KJ, Lohman TM. Kinetic mechanism of adenine nucleotide binding to and hydrolysis by the *Escherichia coli* Rep monomer. 1 Use of fluorescent nucleotide analogues. Biochemistry 1994;33:14550–64. [PubMed: 7981217]
25. Johnson KA. Rapid kinetic analysis of mechanochemical adenosinetriphosphatases. Methods Enzymol 1986;134:677–705. [PubMed: 2950300]
26. Hackney DD, Rosen G, Boyer PD. Subunit interaction during catalysis: alternating site cooperativity in photophosphorylation shown by substrate modulation of [^{18}O]ATP species formation. Proc Natl Acad Sci U S A 1979;76:3646–50. [PubMed: 291029]
27. Olivares AO, Chang W, Mooseker MS, Hackney DD, De La Cruz EM. The tail domain of myosin Va modulates actin binding to one head. J Biol Chem 2006;281:31326–36. [PubMed: 16921171]
28. Hackney DD, Stempel KE, Boyer PD. Oxygen-18 probes of enzymic reactions of phosphate compounds. Methods Enzymol 1980;64:60–83. [PubMed: 7374458]
29. Wong I, Lohman TM. A two-site mechanism for ATP hydrolysis by the asymmetric Rep dimer P2S as revealed by site-specific inhibition with ADP-A1F$_4$. Biochemistry 1997;36:3115–25. [PubMed: 9115987]
30. Yengo CM, De la Cruz EM, Safer D, Ostap EM, Sweeney HL. Kinetic characterization of the weak binding states of myosin V. Biochemistry 2002;41:8508–17. [PubMed: 12081502]
31. De La Cruz EM, Wells AL, Rosenfeld SS, Ostap EM, Sweeney HL. The kinetic mechanism of myosin V. Proc Natl Acad Sci U S A 1999;96:13726–31. [PubMed: 10570140]
32. John, L.; Ingraham, FCN. Escherichia Coli and Salmonella Typhimurium: Cellular and Molecular Biology. ASM Press; Washington, D.C.: 1987.
33. Shi H, Cordin O, Minder CM, Linder P, Xu RM. Crystal structure of the human ATP-dependent splicing and export factor UAP56. Proc Natl Acad Sci U S A 2004;101:17628–33. [PubMed: 15585580]
34. Sengoku T, Nureki O, Nakamura A, Kobayashi S, Yokoyama S. Structural basis for RNA unwinding by the DEAD-box protein *Drosophila* Vasa. Cell 2006;125:287–300. [PubMed: 16630817]
35. Henn A, Shi SP, Zarivach R, Ben-Zeev E, Sagi I. The RNA Helicase DbpA Exhibits a Markedly Different Conformation in the ADP-bound State When Compared with the ATP- or RNA-Bound States. J Biol Chem 2002;277:46559–46565. [PubMed: 12324462]

36. Phillips RC, George P, Rutman RJ. Thermodynamic data for the hydrolysis of adenosine triphosphate as a function of pH, Mg^{2+} ion concentration, and ionic strength. J Biol Chem 1969;244:3330–42. [PubMed: 5792663]
37. Jencks WP. The utilization of binding energy in coupled vectorial processes. Adv Enzymol Relat Areas Mol Biol 1980;51:75–106. [PubMed: 6255774]
38. Xia T, SantaLucia J Jr. Burkard ME, Kierzek R, Schroeder SJ, Jiao X, Cox C, Turner DH. Thermodynamic parameters for an expanded nearest-neighbor model for formation of RNA duplexes with Watson-Crick base pairs. Biochemistry 1998;37:14719–35. [PubMed: 9778347]
39. Tsu CA, Kossen K, Uhlenbeck OC. The *Escherichia coli* DEAD protein DbpA recognizes a small RNA hairpin in 23S rRNA. RNA 2001;7:702–9. [PubMed: 11350034]
40. Gill SC, von Hippel PH. Calculation of protein extinction coefficients from amino acid sequence data. Anal Biochem 1989;182:319–26. [PubMed: 2610349]
41. Henn A, De La Cruz EM. Vertebrate myosin VIIb is a high duty ratio motor adapted for generating and maintaining tension. J Biol Chem 2005;280:39665–76. [PubMed: 16186105]
42. De La Cruz EM, Sweeney HL, Ostap EM. ADP inhibition of myosin V ATPase activity. Biophys J 2000;79:1524–9. [PubMed: 10969013]
43. Brune M, Hunter JL, Corrie JE, Webb MR. Direct, real-time measurement of rapid inorganic phosphate release using a novel fluorescent probe and its application to actomyosin subfragment 1 ATPase. Biochemistry 1994;33:8262–71. [PubMed: 8031761]
44. Samizo K, Ishikawa R, Nakamura A, Kohama K. A highly sensitive method for measurement of myosin ATPase activity by reversed-phase high-performance liquid chromatography. Anal Biochem 2001;293:212–5. [PubMed: 11399034]
45. Barshop BA, Wrenn RF, Frieden C. Analysis of numerical methods for computer simulation of kinetic processes: development of KINSIM--a flexible, portable system. Anal Biochem 1983;130:134–45. [PubMed: 6688159]
46. Gutfreund, H. Kinetics for the Life Sciences: Receptors,transmitters and catalysts. Cambridge University Press; Cambridge: 1995.

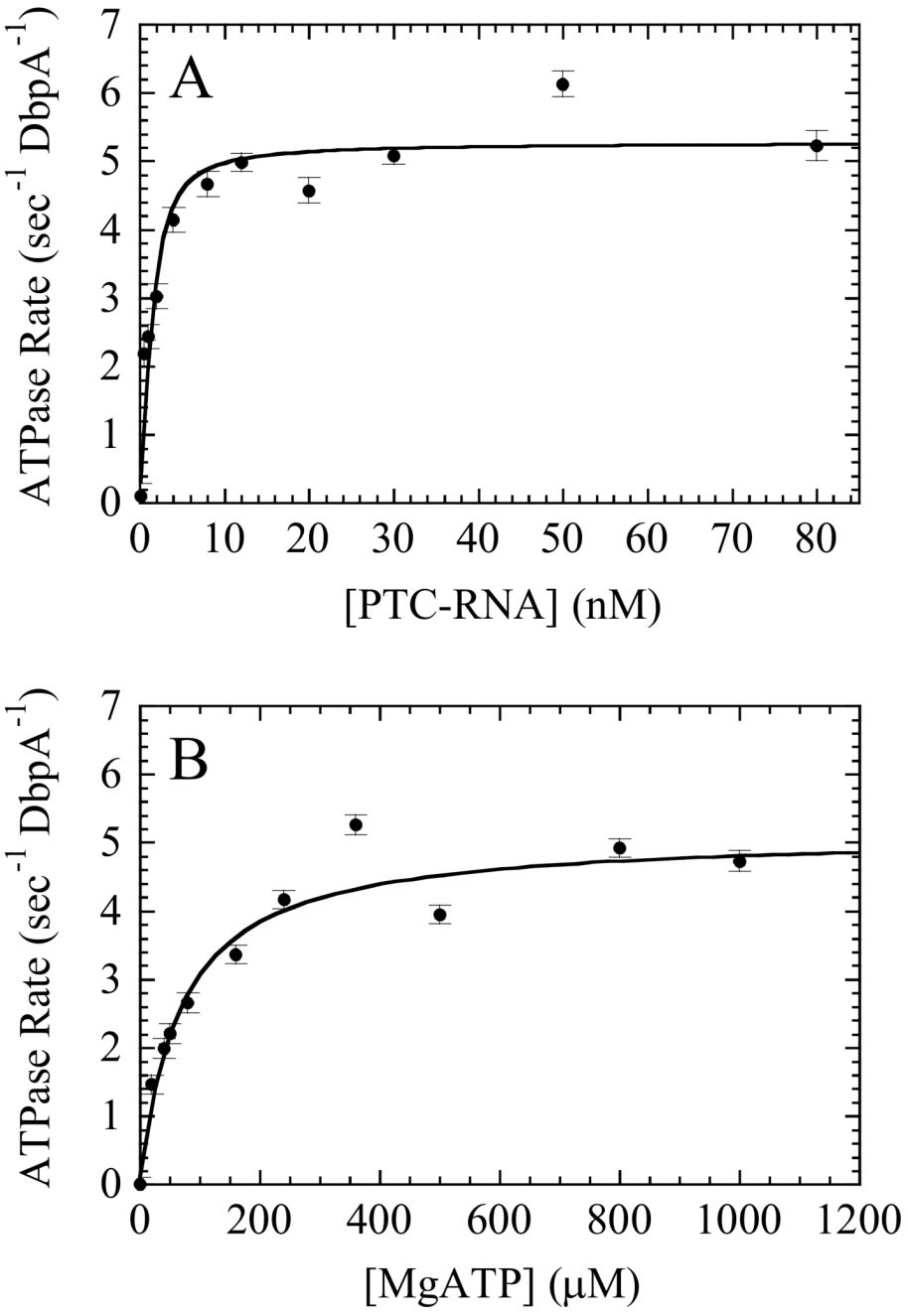

Figure 1. Steady state ATPase activity of DbpA

A. PTC-RNA concentration-dependence of DbpA steady state turnover velocity at saturating (2 mM) ATP. B. ATP concentration-dependence of DbpA steady-state turnover velocity at saturating (120 nM) PTC-RNA. The solid lines through the data points are the best fits to Eq. 9. Uncertainty bars represent the standard errors from the fits. The steady-state ATPase rate is presented as the number of ATP molecules hydrolyzed per DbpA per second.

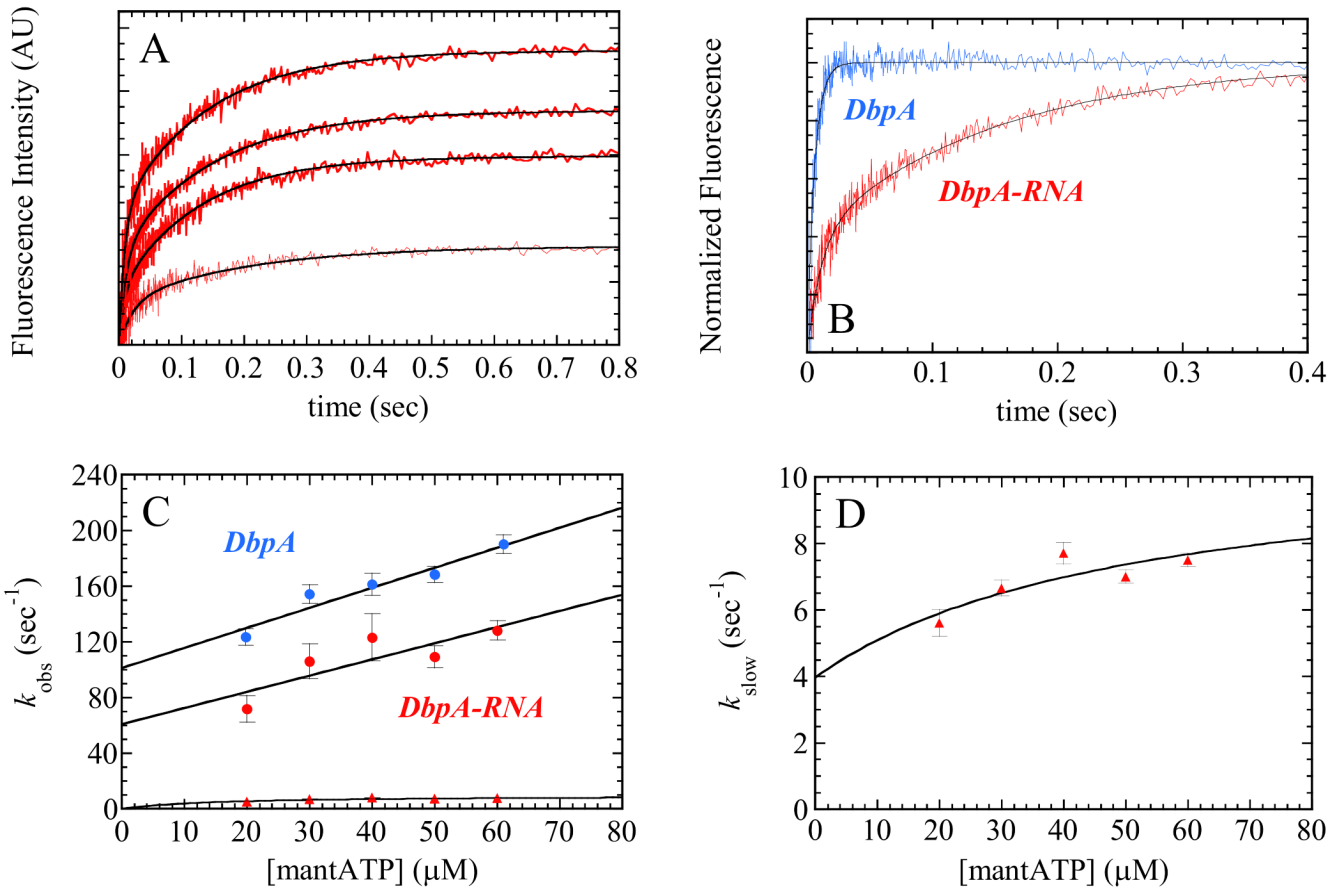

Figure 2. Kinetics of mantATP binding to DbpA and DbpA·PTC-RNA

A. Time courses of mantATP binding assayed by resonance energy transfer from DbpA tryptophans to bound mantATP. The smooth lines through the data represent the best fits to double exponentials. Final concentrations: 1 μM DbpA-PTC-RNA and (*lower to upper*) 30 μM, 40 μM, 60 μM and 100 μM mantATP. B. Time course of 50 μM mantATP binding to 1 μM DbpA (*green*) or 1 μM DbpA·PTC-RNA (*blue*). The solid lines are the best fits to single (DbpA) or double (DbpA-PTC) exponentials. C. [mantATP]-dependence of the fast observed rate constant of binding to DbpA (•) or DbpA·PTC (•). Solid lines are the fits to Eq. 33 of Appendix.. D. [mantATP]-dependence of the slow observed rate constant for binding to DbpA·PTC-RNA (•). The solid line represents the best fit to Eq. 34 of Supplementary Material with the apparent K_d constrained to 51 μM as predicted from the ratio of the rate constants determined from data in Panel C. Uncertainty bars represent standard errors in the fits.

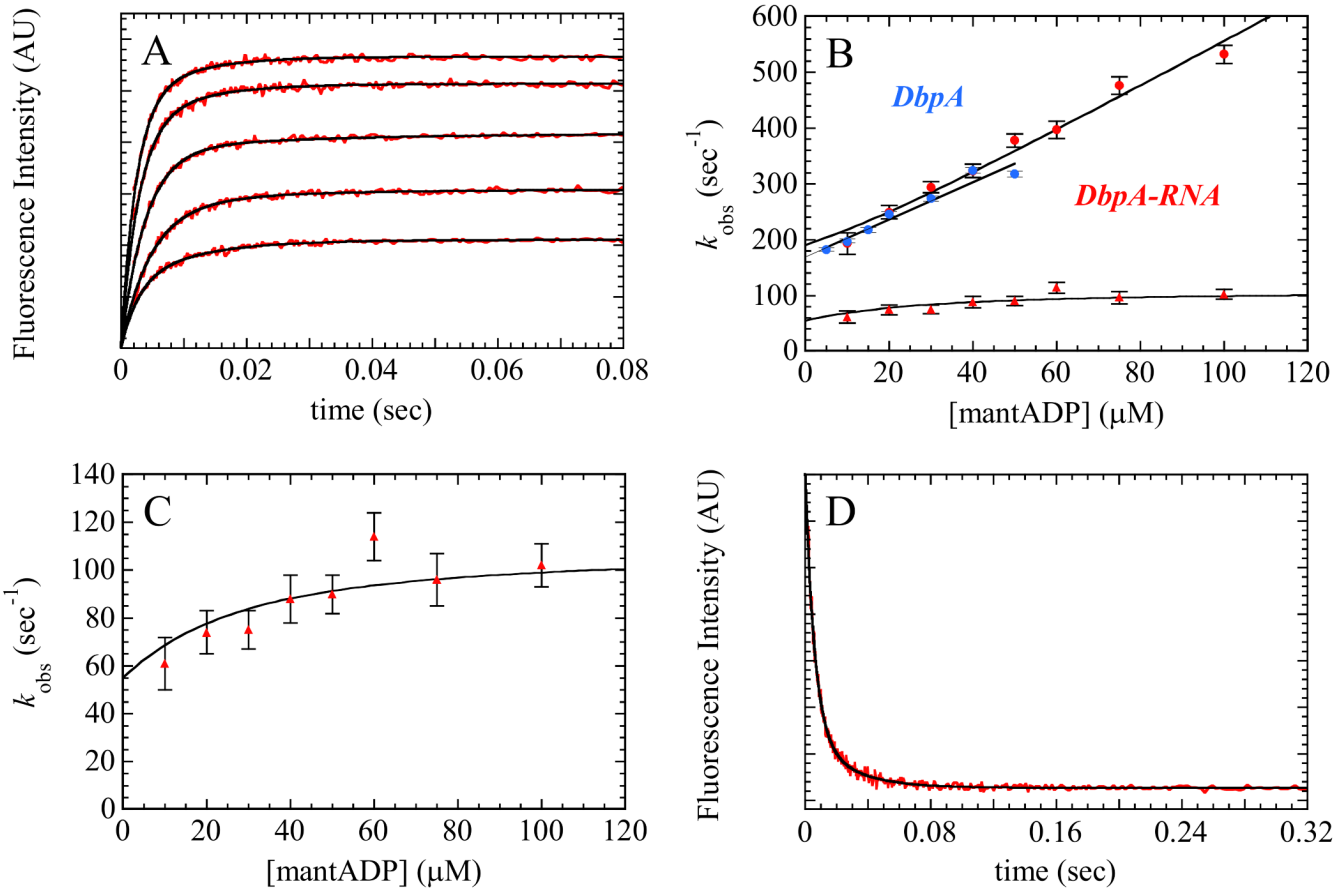

Figure 3. Kinetics of mantADP binding to DbpA-PTC-RNA

A. Time courses of mantADP binding assayed by resonance energy transfer from DbpA tryptophans to bound mantADP. The smooth lines through the data represent the best fits to double exponentials. Final concentrations: 1 μM DbpA·PTC-RNA and (*lower to upper*) 10 μM, 20 μM, 30 μM, 40 μM and 60 μM mantADP. B. [mantATP]-dependence of the observed rate constant binding to DbpA and DbpA·PTC (fast phase (•) and slow phase (▲)). Both solid lines are the fits to Eq. 2. C. The [mantADP]-dependence of the slow observed rate constant of binding mantADP to DbpA-PTC-RNA. Uncertainty bars represent standard errors in the fits. The solid line is the best fit to Eq. 2. D. Time course of mantADP dissociation from DbpA-PTC-RNA after mixing an equilibrated sample of 1 μM DbpA-PTC-RNA and 125 μM mantADP with 2 mM MgADP. The smooth lines are the best fits of the data to double exponentials with a fast observed rate constant of 169.8 (± 4.5) s^{-1} comprising 82% of the amplitude and a slow observed rate constant of 39.7 (± 2.7) s^{-1}.

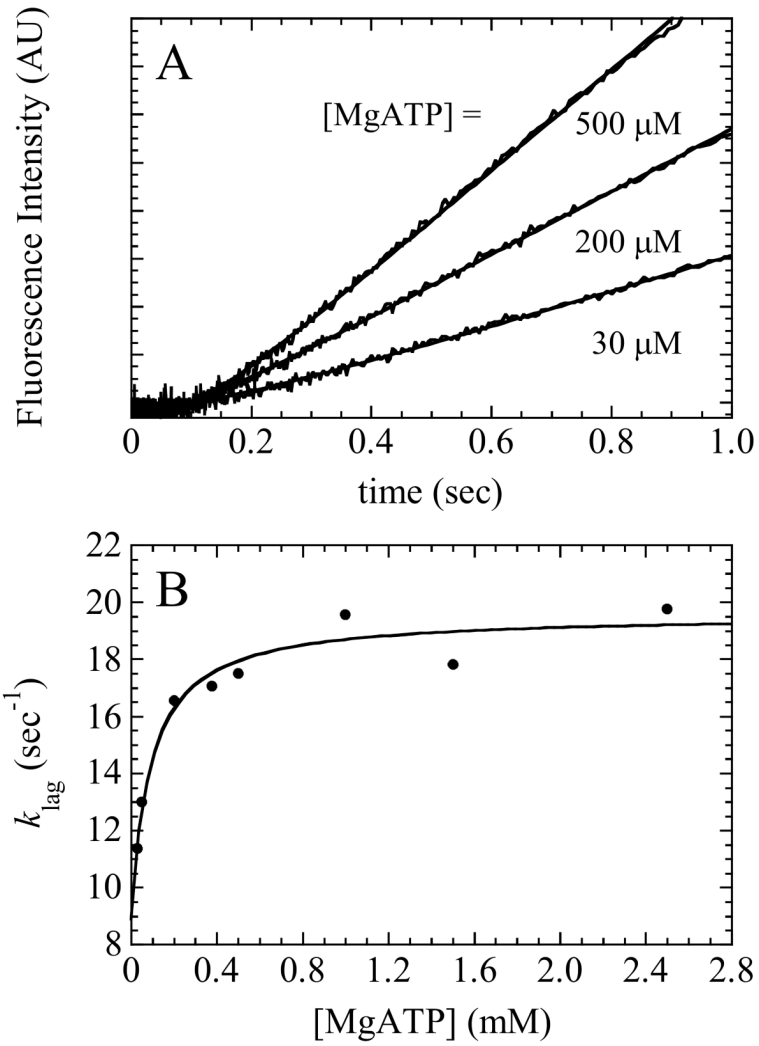

Figure 4. Transient kinetics of P_i release from DbpA-PTC-RNA

A. Time courses of transient P_i release after mixing 1 μM DbpA-PTC-RNA with excess ATP in the presence of 5 μM (final) MDCC-P_iBiP. Solid lines are the best fits to Eq. 38 in Appendix. B. [ATP]-dependence of the observed rate constant that describe the lag phase component of the time courses. The solid line is the fit using Eq. 6.

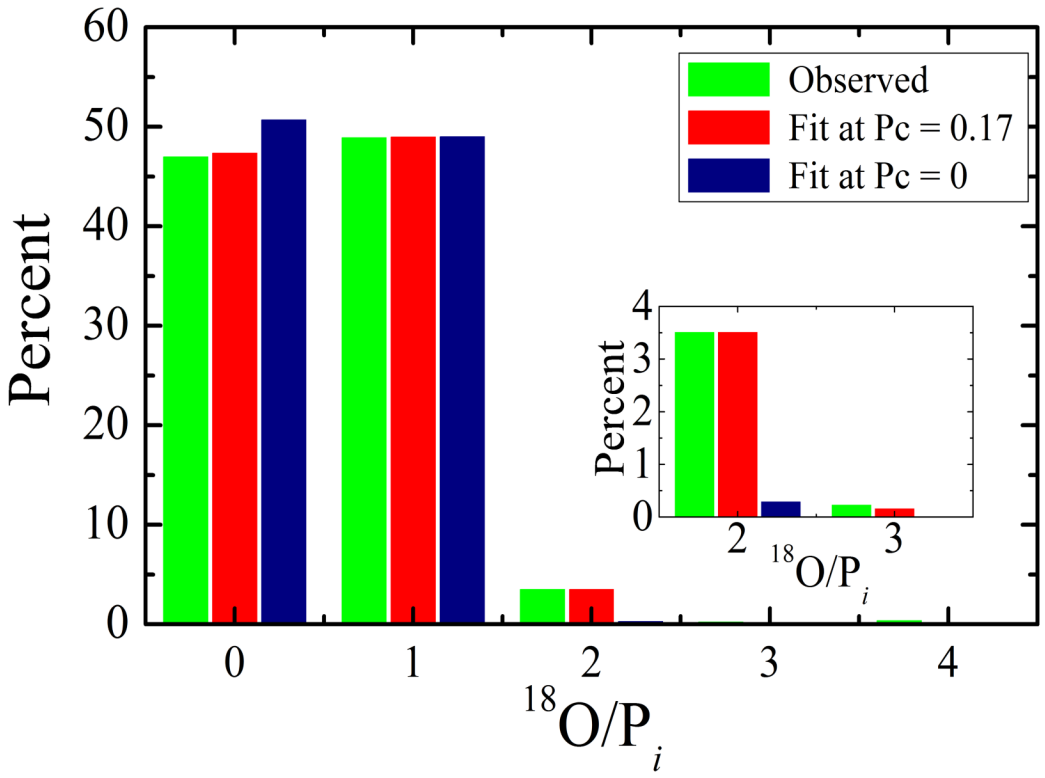

Figure 5. Distribution of ^{18}O-labeled P_i species after hydrolysis of ATP by DbpA-PTC-RNA in 49% ^{18}O-water

Inset-Distribution of ^{18}O-2 and ^{18}O-3 species. Note that only a trace of ^{18}O-3 species due to natural abundance will be detected if there was no exchange.

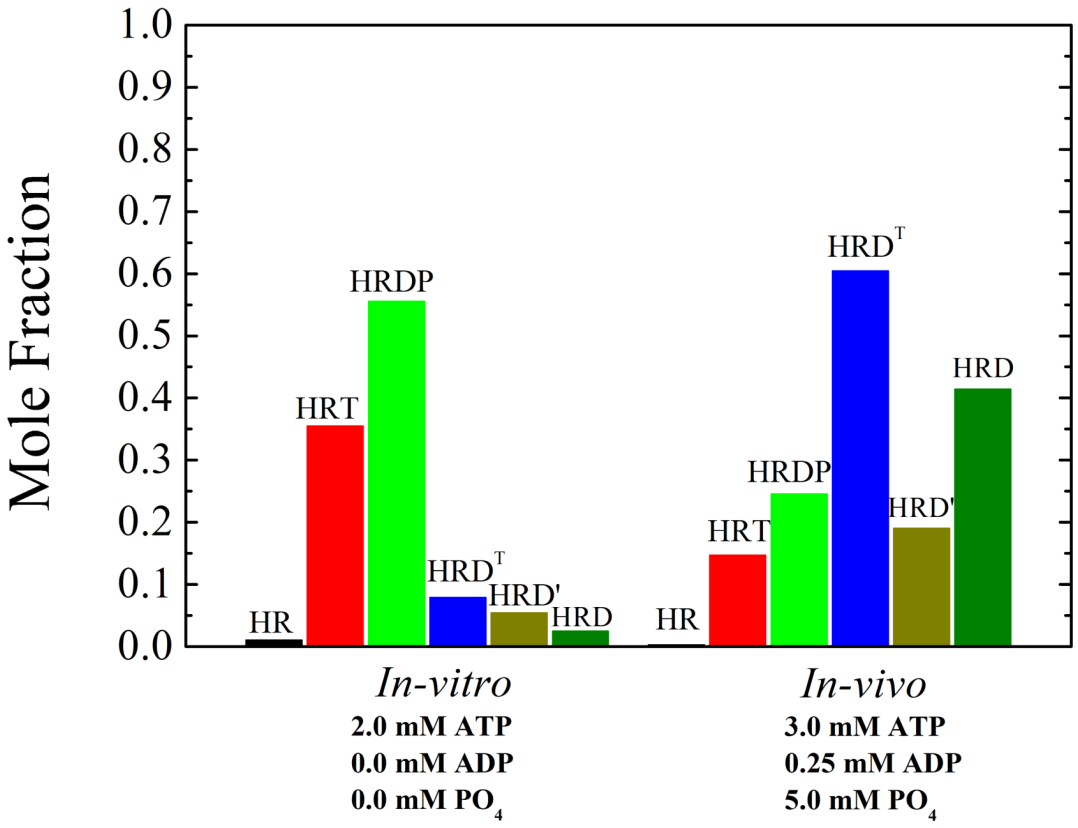

Figure 6. Distribution of the DbpA-RNA biochemical states populated during steady-state ATP cycling

HR represents DbpA- RNA complex, HRT represents DbpA- RNA-ATP, $HRDP_i$ represents DbpA-RNA-ADP-P_i, and HRD^T represents the sum of both DbpA-RNA-ADP states depicted in Scheme 1.

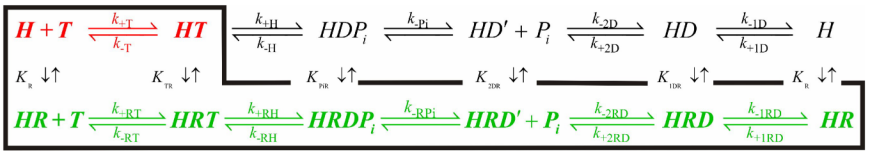

Scheme 1. The rRNA-activated DbpA ATPase cycle

The predominant cycling pathway at saturating rRNA is highlighted in green. The intermediates populated in the absence of RNA are colored red.

Table 1

Rate and equilibrium[a] constants of the DbpA ATPase cycle. [b]

Steady-state parameters		
k_{cat} (-PTC)	< 0.01 s^{-1}	(NADH assay, Figure 1A)
k_{cat} (+PTC)	5.3 (± 0.2) s^{-1}	(NADH assay, Figure 1A)
	5.2 (± 0.3) s^{-1}	(NADH assay, Figure 1B)
k_{cat} (+PTC), predicted	4 s^{-1}	(Equation 8)
$K_{m, ATP}$ (+PTC)	65 (± 14) μM	(NADH assay, Figure 1B)
	82 (± 33)	(P_iBiP, Figure 4)
$K_{m, ATP}$ (+PTC) predicted	23 μM	(Equation 8)
$K_{m, PTC}$	1.0 (± 0.3) nM	(NADH assay, Figure 1A)
$K_{m, PTC}$, predicted	5.2 nM	(Equation 8)
ATP binding		
k_{+T}	1.4 (± 0.2) μM^{-1} s^{-1}	(mantATP; Figure 2C)
k_{-T}	101 (± 7) s^{-1}	(mantATP; Figure 2C)
K_T	72 (± 11) μM	(mantATP, ratio of rate constants)
k_{+RT}	1.2 (± 0.4) μM^{-1} s^{-1}	(mantATP; Figure 2C)
k_{-RT}	61 (± 19) s^{-1}	(mantATP; Figure 2C)
K_{RT}	51 (± 23) μM	(mantATP ratio of rate constants)
	86 (± 56) μM	(ATP, P_iBiP, $K_{0.5}$ of lag, Figure 4B)
Hydrolysis & P_i release		
K_H	≫ 1	(P_iBiP sequential mixing, quench flow)
$k_{+RH} + k_{-RH} + k_{-RPi}$	19.5 (± 4.1) s^{-1}	(P_iBiP; Figure 4B)
	10.8 (± 3.6) s^{-1}	(mantATP slow rate maximum; Figure 2D)
$P_c = k_{-RH}/(k_{-RH} + k_{-RPi})$	0.2	(^{18}O Exchange)
k_{+RH}	11.9 s^{-1}	(^{18}O Exchange & P_i release)
k_{-RH}	1.5 s^{-1}	(^{18}O Exchange & P_i release)
K_{RH}	0.13	(^{18}O Exchange & P_i release)
k_{-RPi}	6.1 s^{-1}	(P_iBiP & ^{18}O Exchange; Figure 4B)
k_{+RPi}	<0.06 mM^{-1} s^{-1}	(calculated from K_{RPi} and k_{-RPi})
K_{RPi}	> 100 mM	(effect of P_i on mantADP release)
K_{Pi}	> 100 mM	(effect of P_i on mantADP release)
ADP binding		
k_{+1D}	3.3 (± 0.3) μM^{-1} s^{-1}	(mantADP; Figure 4B)
k_{-1D}	170 (± 10) s^{-1}	(mantADP; Figure 4B)
	130 (± 2) s^{-1}	(mantADP dissociation time course; Figure 4B)
K_{1D}	51 (± 6) μM	(mantADP ratio of rate constants Figure 4B)
K_{2D}	≫1	(no slow phase in mantADP binding)
k_{+1RD}	4.1 (± 0.2) μM^{-1} s^{-1}	(mantADP; Figure 4B)
k_{-1RD}	137 (± 20) s^{-1}	(mantADP; Figure4B)
K_{1RD}	33 (± 5) μM	(mantADP ratio of rate constants; Figure 4B)
k_{+2RD}	32 (± 18) s^{-1}	(mantADP; Figure 4C)
k_{-2RD}	77 (± 10) s^{-1}	(mantADP; Figure 4C)
K_{2RD}	2.4 (± 1.3)	(mantADP; Figure 4C)
$K_{RD, overall}$	23 (± 4) μM	(mantADP; Equation 3)
RNA binding[c]		
$K_{R, overall}$	16 (± 2) nM	(EMSA, data not shown)
$K_{TR, overall}$ [d]	11 nM	(calculated from detailed balance)
$K_{PiR, overall}$ [e]	≪ 1.5 nM	(estimated from detailed balance)
$K_{2DR, overall}$ [f]	≪25 nM	(estimated from detailed balance)
$K_{1DR, overall}$ [g]	10 nM	(calculated from detailed balance)

[a] K_i defined as k_{-i}/k_{+i}

[b] Conditions: 75 mM KCl, 20 mM K-HEPES (pH 7.5), 5 mM $MgCl_2$, 1 mM DTT, 25 °C.

[c] K_i represent dissociation equilibrium constants for overall PTC-RNA binding

[d] Calculated from $K_{TR} = K_{RT} K_R/K_T$

[e] Calculated from $K_{PiR} = K_{TR} K_{RH}/K_H$

[f] Calculated from $K_{2DR} = K_{1DR} K_{2RD}/K_{2D}$

[g] Calculated from $K_{1DR} = K_{1RD} K_R/K_{1D}$

Table 2

Equilibrium constants and standard Gibbs free energy changes associated with DbpA, PTC-RNA (153 mer) and nucleotide association at 25 °C

	K_d	$\Delta G^{o'}_{assoc}$ (kJ mol^{-1})
K_T	72 μM	-23.6
K_{RT}	51 μM	-24.5
K_H	≫ 1	≫ 0
K_{RH}	0.13	-5.1
K_{Pi}	> 100 mM	< 5.7
K_{RPi}	> 100 mM	< 5.7
K_{2D}	≫ 1	≫ 0
K_{2RD}	2.4	2.2
K_{1D}	51 μM	-24.5
K_{1RD}	33 μM	-25.6
K_R	16 nM	-44.5
K_{TR}	11 nM	-45.3
K_{PiR}	≪ 1.5 nM	≪ -50.4
K_{1DR}	10 nM	-45.6
K_{2DR}	≪ 25 nM	≪ -43.4

$K_{1DR} = K_{1RD}\,K_R/K_{1D}$

$K_{TR} = K_{RT}\,K_R/K_T$

$K_{PiR} = K_{TR}\,K_{RH}/K_H$

$K_{2DR} = K_{1DR}\,K_{2RD}/K_{2D}$